Generalized autocorrelation function in the family of deterministic and stochastic anomalous diffusion processes

Muhammad Tayyab ⬡*

School of Computing Sciences, Pak-Austria Fachhochschule Institute of Applied Sciences and Technology, Mang, 22621 Haripur, Pakistan
and Faculty of Engineering Sciences, Ghulam Ishaq Khan Institute of Engineering Sciences and Technology, Topi, 23640 Swabi, Pakistan

We investigate the observables of the one-dimensional model for anomalous transport in semiconductor devices where diffusion arises from scattering at dislocations at fixed random positions, known as the Lévy-Lorentz gas. To gain insight into the microscopic properties of such a stochastically complex system, deterministic dynamics known as the slicer map and fly-and-die dynamics are used. We analytically derive the generalized position autocorrelation function of these dynamics and study the special case, the 3-point position correlation function. For this, we derive single-parameter-dependent scaling and compare it with the numerically estimated 3-point position autocorrelation of the Lévy-Lorentz gas, for which the analytical expression is still an open question. Here we obtained a remarkable agreement between them, irrespective of any functional relationship with time. Moreover, we demonstrate that the position moments and the position autocorrelations of these systems scale in the same fashion, provided the times are large enough and far enough apart. Other observables, such as velocity moments and correlations, are reported to distinguish the systems.

I. INTRODUCTION

Anomalous transport has been a very active field of research for several decades, but in the past few years it has received enormous attention due to its potential application in numerous fields of science that describe many physical phenomena. For instance, this has been observed in charge carrier motion in semiconductors [1], in polygonal billiards [2,3], in ion motion within electrolytic cells [4], in single molecules inside living cells [5], in ultracold atoms [6], in disordered media [7], in artificially crowded systems and protein-crowded lipid bilayer membranes [8–10], in experimental evidence on the mobility of particles in living cancer cells [11], and in many other cases.

The one quantity of interest to study is transport exponent γ for which the generalized diffusion coefficient,

$$D_\gamma = \lim_{n\to\infty} \frac{\langle (x_n - x_0)^2 \rangle}{n^\gamma} \in (0, \infty), \qquad (1)$$

is positive and finite. The numerator $\langle (x_n - x_0)^2 \rangle$ represents the mean square displacement (MSD) for the position of particle x_n at time n. The angular brackets $\langle \cdot \rangle$ correspond to the ensemble average over all particles. The exponent γ takes the values $0 \leqslant \gamma \leqslant 2$; the transport is called subdiffusive for $0 \leqslant \gamma < 1$, which leads to rapid limit decay; it is called

standard diffusion for $\gamma = 1$ followed by Fick's law, which has the basic characteristic that the MSD grows linearly in time; and it is called superdiffusive when $1 < \gamma < 2$, and hence the limit diverges, and $\gamma = 2$ yields ballistic diffusion. Collectively, except for $\gamma = 1$, this represents a wide spectrum, commonly known as anomalous transport [12–18]. A contemporary summary of a rich variety of anomalous diffusion processes is provided in [19], whereas standard diffusion has been widely investigated in the literature, for instance, see [18,20–22] and references therein. Dynamical systems that exhibit all possible diffusion regimes in the field of anomalous transport are rare in the literature, although in the realm of deterministic dynamics, several authors have investigated anomalous diffusion [2,3,23]. Moreover, in the era of deterministic dynamics, the transport phenomenon is well understood in chaotic systems, which commonly corresponds to standard diffusion. This has happened due to the fast rate at which correlation decays. In nonchaotic systems, transport is still underlying, which may often lead to anomalous transport. This is since the rate at which correlation decays is much slower [3,14,17,18,24,25]. In the presence of stochastic elements, the scenario is often closer to that of chaotic dynamics [26,27], but numerous questions remain open [16,18,25,28–35]. In particular, the asymptotic behavior of correlation functions is not understood in general, although it is relevant, e.g., to distinguish transport processes that are effectively different but have the same moments [30]. Numerous investigations have been devoted to this subject; see, e.g., [36–41].

The slicer map (SM) was introduced by Salari *et al.* [24] to study mass transport. The original point of interest was to construct an exactly solvable model (perfect determinism) that would reproduce the transport regimes found numerically in polygonal billiards [3]. The SM diffuses in one scaling

---

*Contact author: muhammad.tayyab@fecid.paf-iast.edu.pk

regime and exhibits sub-, super-, and normal diffusion under a single parameter variation. The position statistics of the SM, including many systems that exhibit strong anomalous transport, are dominated by ballistic trajectories [42–45]. It has been proven by Salari *et al.* [24] that the SM regenerates the asymptotic scaling of the position moments of a much more complex system, the Lévy-Lorentz gas (LLG) [29,35]. The LLG is a one-dimensional random walk in a random environment in which the scatterers are randomly distributed on a line according to a Lévy-stable probability distribution. Burioni *et al.* [35] used simplifying assumptions to determine the mean square displacement of the traveled distance and numerically validated their findings. More recently, Bianchi *et al.* [46] presented a rigorous mathematical study to prove a central limit theorem, and Zamparo [47] investigated large fluctuations and transport properties of the LLG. It was further proven by Giberti *et al.* [48] that when the single parameters α and ξ of the SM and the LLG, respectively, are properly tuned, this choice of parameters leads, within the transport regimes of the LLG, to the equality of the asymptotic scalings of the 2-point position autocorrelation functions. This makes two very different systems indistinguishable regardless of their microscopic dynamics, as far as the statistics of positions are concerned. Indeed, such an agreement does not infer a full equivalence of the dynamics. For example, the trajectories of the SM move ballistically in an initial transit and then turn periodic in a period-2 cycle, then remain oscillating back and forth between their neighboring cells, while in the LLG all trajectories are stochastic. This fact is further addressed in Secs. II A and IV.

The deterministic and time-continuous prototypical model, fly-and-die (FND) dynamics, was introduced to mimic the universal features of displacement statistics [42]. The FND dynamics exhibit a wide spectrum of diffusion, from sub- to normal to superdiffusion, upon varying a single parameter. In the FND, strong anomalous diffusion (superdiffusion) emerges due to ballistic trajectories, i.e., the ballistic trajectories that did not undergo transitions up to any finite time (see for instance [49]). It is further motivated by the fact that subdominant terms in the FND and the SM contribute like ballistic flights to the asymptotic behavior; i.e., they contribute the maximum allowed for a system to belong to the universal behavior. This is further proven by the fact that, analytically, all the position moments and the 2-point position correlations of the FND asymptotically scale as those of the SM despite having different microscopic structures. Upon tuning the diffusion parameter of the SM and the FND with the LLG in accordance with this agreement, all the moments coincide analytically and with remarkable numerical agreement. At the same time, the 2-point position correlation exhibits the same power-law behavior as those numerically estimated position correlations in the LLG [42,48].

In this paper, we intend to explore the equivalence of the higher-order position autocorrelation function of the SM, the FND, and the LLG and see up to which order of correlation the SM and the FND are indistinguishable from the LLG. For this, first, we derive the generalized position autocorrelation function of the SM and the FND, and then, for the particular case, i.e., the 3-point position autocorrelation function, we compute a single scaling form that depends only

on one parameter: h_2/n_2 [cf. Eqs. (12) and (31)], which is simply the ratio of times. We compare one parameter-dependent analytical scaling form of correlation with the numerically estimated position autocorrelation function of the much more realistic model, the LLG. We find remarkable agreement between the correlation scaling of the SM, the FND, and all numerically estimated 3-point position correlations of the LLG. Regardless of any functional relationship between the time, all data sit on top of each other and have a nice agreement with the theoretical prediction [cf. Eqs. (12) and (31)]. Moreover, the velocity moments and correlation function are also reported to observe the dissimilarities in these systems. On the contrary, we also argue about the statistics of the position moments and the correlations that scale in the same way; see Fig. 3. This is due to the fact that, in the correlation function, separation between different times becomes irrelevant as compared to the mean.

This paper is organized as follows: Sec. II A formally summarizes the SM and illustrates its properties. Section II A 2 provides the m-point position autocorrelation function expression. Section II A 3 demonstrates a scaling formula for the 3-point position autocorrelation function. In Secs. II A 4 and II A 5, we formally introduce velocity moments and correlation functions of the SM. Section II B does the same for the FND dynamics. Section III A devotes itself to the LLG, which characterizes the properties of the system and also reports numerical results on the applicability of the scaling formula for the 3-point position autocorrelations. Section IV summarizes our conclusions.

II. DETERMINISTIC DYNAMICS

A. The slicer map

The SM is one-dimensional, deterministic, and exactly solvable dynamics [24,48]. Its time evolution is given by the map

$$S_\alpha : [0, 1] \times \mathbb{Z} \to [0, 1] \times \mathbb{Z}$$

defined by (see Fig. 1)

$$x_{n+1} = S_\alpha(x_n)$$

$$= \begin{cases} (x_n, m - 1) & \text{if } 0 \leqslant x_n \leqslant \ell_m \text{ or } \frac{1}{2} < x_n \leqslant 1 - \ell_m, \\ (x_n, m + 1) & \text{if } \ell_m < x_n \leqslant \frac{1}{2} \text{ or } 1 - \ell_m < x_n \leqslant 1. \end{cases}$$
(2a)

Here $x_n = \{x + n\}$, where x is the fractional part (i.e., $0 \leqslant x < 1$) and $n \in \mathbb{N}_0$ a non-negative integer. In each term x_n, n is added to x, and the use of the fractional part function ensures that x_n remains within the interval [0,1]. The initial ensemble x_0 is chosen uniformly in the interval [0,1].

The family of slicers

$$\ell_m = \frac{1}{(|m| + 2^{1/\alpha})^\alpha}, \qquad \text{with } \alpha \in \mathbb{R}^+, \qquad (2b)$$

determines the position of the slicer and chops the slices in their neighboring cells.

For $1/2 < x_n < 1$ each iteration of the map increases the values of m by 1, until $x_n > \ell_m$. Subsequently, the trajectory enters a stable period-2 cycle, oscillating back and forth between the two neighboring sites m and $m - 1$. Similarly, for
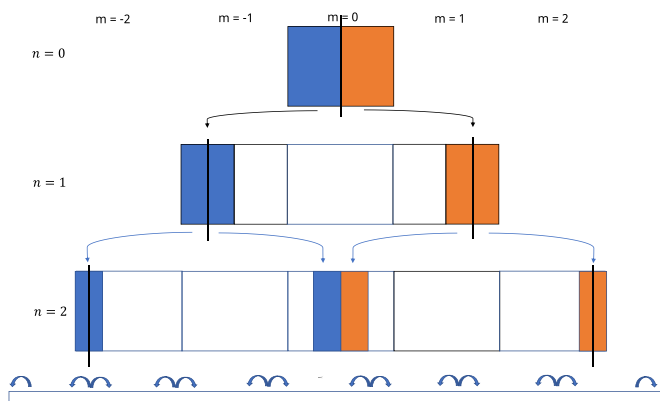
FIG. 1. Demonstration of space-time plot for the slicer map defined by S_α in Eq. (2), where n represents time and m space; shown is the diffusive spreading of points that at $n = 0$ are uniformly distributed initial condition on the unit interval centered around $m = 0$. Iteration of the map S_α is shown up to time $n = 2$; it represents that points in the centered cell $m = 0$ start moving in their neighboring cells as n grows. The lower horizontal strip with back-and-forth signs on the central and forward-backward signs on the edges denotes sub-traveling and traveling points, respectively, as n grows.

$0 < x_n < 1/2$ each iteration of the map decreases the values of m by 1 until $x_n < -\ell_m$, and then the trajectory enters a stable period-2 cycle. The distance between two trajectories does not change in time, as long as they are mapped by the same branch of the map which, for each $m \in \mathbb{Z}$, is defined by the "slicer" ℓ_m. The distance between two points x_n and x_{n+1} jumps discontinuously when they reach a cell m where $\ell_m \in [x_n, x_{n+1}]$. Thus, the dynamics is reminiscent of polygonal billiard dynamics [2,3], where initial conditions are only separated when they are reflected by different sides of the polygon. The corners act as slicers of the bundle of initial conditions. The analogy between the two systems also includes the fact the SM has a vanishing Lyapunov exponent and it preserves the phase space volume. Likewise the SM exhibits sub-, super-, and normal diffusion upon varying the parameter α that describes the position of the slicers (see [24,48] and references therein). Therefore such deterministic dynamics are rare in the literature of transport processes that shows a wide spectrum of diffusion.

1. pth position moments

Salari *et al.* [24] introduced the SM and calculated all moments of the displacement as a function of the number n of iterations of the map. In the following, we review those calculations differently, but for the sake of simplest representation, we shift the origin of the positions by $1/2$, so that the right half of the unit interval coincides with $[0, 1/2]$, rather than $[1/2, 1]$. This does not affect the asymptotic results that are obtained from an ensemble of initial conditions with $m = 0$ and x_0 uniformly distributed in the right half of the unit interval. For $n \gg 2^{1/\alpha}$ the pth position moments amount to following Lemma 1.

Lemma 1. Given $\alpha > 0$, the pth position moments of the slicer dynamics for uniformly distributed initial conditions

asymptotically scale as

$$\langle (x_n - x_0)^p \rangle \sim \begin{cases} \text{constant,} & \text{for } p < \alpha, \\ 2 \ln \frac{n^\alpha}{2}, & \text{for } p = \alpha, \\ \frac{2p}{p-\alpha} n^{p-\alpha}, & \text{for } p > \alpha > 0. \end{cases} \quad (3)$$

Proof. See Appendix A 1. ■

For $p = 2$, the MSD $\langle (x_n - x_0)^2 \rangle \sim n^\gamma$, where $\gamma = 2 - \alpha$ with $0 < \gamma < 2$, captures all scenarios of anomalous diffusion. The SM exhibits superdiffusion for $\gamma > 1$; for $\gamma = 1$, the power law grows linearly in time, i.e., it is normal diffusive; and for $\gamma < 1$, it is subdiffusive. Since there is no drift in the SM, all odd moments vanish. Once we confine the motion of particles in one direction, we can also identify all odd position moments.

The 2-point position autocorrelation function of the SM asymptotically scales as those of the numerically estimated position correlations of the LLG [48]. Since our fundamental objective is to observe the equivalence of the position autocorrelation functions of different dynamics, only partial equivalence at the level of all position moments and the correlation function of order 2 do not suffice to determine the indistinguishability of the dynamics. This may leave many unanswered questions; e.g., as far as the statistics of positions are concerned, one does not know to what extent the SM, the FND, and the LLG are indistinguishable. To address these questions, in the following, we explicitly derive the generalized position autocorrelation function of the SM and the FND to see how far equivalence holds to the numerically estimated correlations of the LLG.

2. Generalized position autocorrelation function

The generalized (or m-point) position autocorrelation function of the SM for time $n_m \geqslant n_{m-1} \geqslant \cdots \geqslant n_2 \geqslant n_1$ is defined as

$$\phi_\alpha(n_1, n_2, \ldots, n_m) = \langle (x_{n_1} - x_0) \cdots (x_{n_{m-1}} - x_0)(x_{n_m} - x_0) \rangle$$

$$= \langle \Delta x_{n_1} \cdots \Delta x_{n_{m-1}} \Delta x_{n_m} \rangle$$

$$= \int_0^{1/2} dx \, \Delta x_{n_1} \cdots \Delta x_{n_{m-1}} \Delta x_{n_m}. \quad (4)$$

According to the flight of trajectories, the integration interval $\mathcal{F} = (0, 1/2)$ is partitioned into $m + 1$ parts, i.e., $\mathcal{F} = L^{>n_m} \cup L^{>n_{m-1}} \cup \cdots \cup L^{>n_1} \cup L^{\geqslant 1/2}$, defined as

$$\phi_\alpha(n_1, n_2, \ldots, n_m) = \int_{L^{>n_m}} dx \, \Delta x_{n_1} \Delta x_{n_2} \cdots \Delta x_{n_m}$$

$$+ \int_{L^{>n_{m-1}}} dx \, \Delta x_{n_1} \Delta x_{n_2} \cdots \Delta x_{n_m}$$

$$+ \cdots + \int_{L^{>n_1}} dx \, \Delta x_{n_1} \Delta x_{n_2} \cdots \Delta x_{n_m}$$

$$+ \int_{L^{\geqslant 1/2}} dx \, \Delta x_{n_1} \Delta x_{n_2} \cdots \Delta x_{n_m}, \quad (5)$$

with $n_m \geqslant n_{m-1} \geqslant \cdots \geqslant n_2 \geqslant n_1$.

The integration limits are separated according to their trajectory flying time:

$L^{>n_m} = \{0 < x < \ell_{n_m}\}$: All trajectories are flying at all times, such that $\Delta x_{n_k} = n_k$, with $k = 1, 2, 3, \ldots, m$.

$L^{>n_{m-1}} = \{\ell_{n_m} < x < \ell_{n_{m-1}}\}$: The trajectory is still flying at time n_{m-1}, but it has localized (turned periodic) by time n_m, and consequently $\Delta x_{n_m} = (x^{-1/\alpha} - 2^{1/\alpha})$ and $\Delta x_{n_k} = \prod_{k=1}^{m-1} n_k$.

$\vdots$

$L^{>n_1} = \{\ell_{n_2} < x < \ell_{n_1}\}$: The trajectory is still flying at time n_1, but it has localized by time n_2 and subsequent;

consequently $\Delta x_{n_1} = n_1$, and $\Delta x_{n_k} = (x^{-1/\alpha} - 2^{1/\alpha})^k$ with $k = 2, 3, \ldots, m-1$.

$L^{\geq 1/2} = \{\ell_{n_1} < x < 1/2\}$: All trajectories get localized before time n_1; hence $\Delta x_{n_k} = (x^{-1/\alpha} - 2^{1/\alpha})^k$ with $k = 1, 2, 3, \ldots, m$.

Therefore for $n_m \geqslant n_{m-1} \geqslant \cdots \geqslant n_2 \geqslant n_1$, integrals emerge as

$$
\phi_\alpha(n_1, n_2, \ldots, n_m) \simeq 2(n_1 n_2 \cdots n_m) \int_0^{\ell_{n_m}} dx + 2(n_1 n_2 \cdots n_{m-1}) \int_{\ell_{n_m}}^{\ell_{n_{m-1}}} dx\, (x^{-\frac{1}{\alpha}} - 2^{\frac{1}{\alpha}})
$$

$$
+ \cdots + 2\, n_1 \int_{\ell_{n_2}}^{\ell_{n_1}} dx(x^{-\frac{1}{\alpha}} - 2^{\frac{1}{\alpha}})^{m-1} + 2 \int_{\ell_{n_1}}^{1/2} dx(x^{-\frac{1}{\alpha}} - 2^{\frac{1}{\alpha}})^m
$$

$$
\simeq 2 \sum_{j=0}^m \left(\prod_{k=1}^{m-j} n_k \int_{\ell_{n_{m-j+1}}}^{\ell_{n_{m-j}}} dx(x^{-\frac{1}{\alpha}} - 2^{\frac{1}{\alpha}})^j \right) \sim 2 \sum_{j=0}^m \left[\prod_{k=1}^{m-j} n_k \left(\frac{\alpha}{\alpha - j} \left(n_{m-j}^{j-\alpha} - n_{m-j+1}^{j-\alpha} \right) \right) \right], \tag{6}
$$

and $n_{m+1} = 0$ and $n_0 = K$, where K is constant.

3. 3-point position autocorrelation function

The 3-point position autocorrelation function can be obtained by requesting $m = 3$ in Eq. (6); the correlation function amounts to

$\phi_\alpha(n_1, n_2, n_3)$

$$
\simeq \begin{cases} \frac{2 n_1 n_2 n_3^{1-\alpha}}{1-\alpha} - \frac{2\alpha\, n_1\, n_2^{2-\alpha}}{(2-\alpha)(1-\alpha)} - \frac{2\alpha\, n_1^{3-\alpha}}{(2-\alpha)(3-\alpha)}, & \alpha \neq 1, \\ 2\, n_2\, n_3 \left(\ln \frac{n_1}{n_2} + 2 \right) + 24 \ln \frac{n_3}{2} - n_3^2 \\ + 8\, n_3 \left(\ln \frac{n_3}{n_2} - 2 \right), & \alpha = 1. \end{cases} \tag{7}
$$

(I) For any fixed time n_1 and for the other two equivalent times $n_2 = n_3$, we recover the asymptotic scaling of the MSD [cf. Eq. (3) with $p = 2$] as given by

$$
\langle (x_n - x_0)^2 \rangle \sim \frac{4}{2-\alpha} n^{2-\alpha}, \quad 0 < \alpha < 2. \tag{8}
$$

(II) For $n_1 = n_2 = n_3$, this reduces to the third moment of displacement [cf. Eq. (3) with $p = 3$], such as

$$
\langle (x_n - x_0)^3 \rangle \sim \frac{6}{3-\alpha} n^{3-\alpha}, \quad 0 < \alpha < 3. \tag{9}
$$

A few cases of the time composition can be defined as follows:

(1) $h_1 = n_2 - n_1$, as $h_1 > 0$, either finite or $h_1 \sim n_1^{q_1}$, $q_1 \leqslant 1$, and $n_1 \to \infty$.

(2) $h_2 = n_3 - n_2$, as $h_2 > 0$ either finite or $h_2 \sim n_1^{q_2}$, $q_2 \leqslant 1$, where $n_2 = n_1 + h_1$, and $n_1 \to \infty$.

(3) $n_1 \geqslant n_2$ are fixed and set $n_3 \to \infty$.

If one sets that all n times tend to infinity for the 3-point position autocorrelation function $\phi_\alpha(n_1, n_2, n_3)$, as given in Eq. (7), the power-law exponent scales in the same way as found for the third position moment (see Lemma 2 for $m = 3$). To address this, we consider the scaling of the correlation $\phi_\alpha(n_1, n_1 + h_1, n_1 + h_1 + h_2)$ for very large values of n_1. For large n_1, when the time lags h_{k-1} are either constant or scale

as $\sim n^q$ for $k = 2, 3$ with $q < 1$, the difference among the three times becomes negligible compared to the mean.

Lemma 2. For $0 < \alpha < m$, as all n times tend to infinity and $h_{k-1} = n_k - n_{k-1}$, for $k = 2, 3, \ldots, m$, where h_{k-1} is either fixed or $\sim n_1^q$, $q < 1$, the m-point position autocorrelation function ϕ_α represented in Eq. (7) asymptotically scales as

$$
\phi_\alpha(n_1, n_2, \ldots, n_m) \sim \frac{2\, m}{m - \alpha} n_1^{m-\alpha}, \quad 0 < \alpha < m. \tag{10}
$$

Proof. This is a direct consequence of Eq. (7). ∎

Remark 1. For $0 < \alpha < m$, where $m = 2$ or 3, as n tends to infinity, the 2- and 3-point position autocorrelation functions $\phi(\alpha)$, following the h_{k-1} represented in Lemma 2, exhibit the same asymptotic scaling as the second moment, i.e., MSD [see Eq. (10)], and the third moment of displacement [see Eq. (9)], which is

$$
\phi_\alpha(n_1, n_2) \sim \langle (x_n - x_0)^2 \rangle, \quad \phi_\alpha(n_1, n_2, n_3) \sim \langle (x_n - x_0)^3 \rangle, \tag{11}
$$

respectively.

For the single-parameter correlation function, we reconsider Eq. (7), rearrange some terms, introduce the time lag $h_2 = n_3 - n_2$ and $h_1 = n_2 - n_1$ and the normalization factor $n_1 n_2^{2-\alpha}$, and find

$$
\phi_\alpha\left(\frac{h_2}{n_2} \right) = \frac{\phi_\alpha(n_1, n_2, n_3)}{n_1 n_2^{2-\alpha}}
$$

$$
\simeq \frac{2}{1-\alpha} \left[\left(1 + \frac{h_2}{n_2} \right)^{1-\alpha} - \frac{\alpha}{2-\alpha} \right.
$$

$$
\left. - \frac{\alpha(1-\alpha)}{(2-\alpha)(3-\alpha)} \left(1 + \frac{h_1}{n_1} \right)^{-(2-\alpha)} \right], \quad \alpha \neq 1. \tag{12a}
$$

For $\alpha < 1$, this scales asymptotically as

$$
\phi_\alpha\left(\frac{h_2}{n_2}\right) \sim \begin{cases} \frac{2}{1-\alpha}\left(\frac{h_2}{n_2}\right)^{1-\alpha}, & \text{for } h_2 \gg n_2, \\ \frac{6}{3-\alpha}, & \text{for } h_2 \ll n_2, \; h_1 \ll n_1, \\ \frac{4}{2-\alpha}, & \text{for } h_2 \ll n_2, \; h_1 \gg n_1. \end{cases}
$$
(12b)

We hence predict a data collapse for the 3-point position autocorrelation when plotting the left-hand side of Eq. (12b) as a function of h_2/n_2. For the regime when $h_2 \gg n_2$, one can observe the power law as $1 - \alpha$, while for $h_2 \ll n_2$, the correlation converges to some constants. Hence, Eq. (12b) provides a new way of analysis for the position autocorrelation function, that depends only on a single parameter h_2/n_2, and the scaling form for different time composition becomes irrelevant [42,48]. The scaling of the 3-point position autocorrelation function captures salient features which are commonly observed in anomalous transport dynamics; for instance when all times n_1, n_2, and n_3 are far separated and large enough, one commonly observes that correlation grows with $n_1 n_2^{2-\alpha}$, like $1/(n_1 n_2^{2-\alpha})$, in accordance with the prediction of Eq. (12b). In Sec. III C we investigate how far these qualitative findings are substantial for quantitative comparison to the LLG [29,35] that does not have mathematical findings on the position autocorrelation function.

4. Moments of velocity

The velocity of any point of the SM is either $+1$ or -1 and moments of the velocity can be determined by evaluating

$$
\langle v^p(n) \rangle = 2 \sum_{k=1}^{n} v_k^p(n) \Delta_k(\alpha) + 2 \sum_{k=n+1}^{\infty} v_k^p(n) \Delta_k(\alpha), \quad (13)
$$

where $v_k(n)$ is the velocity at time n of particle with $x \in [\ell_{k-1}^+, \ell_k^+)$ where $\ell_k^+ = 1 - \ell_k$ and $\Delta_k(\alpha) = \ell_k^+ - \ell_{k-1}^+ = \alpha/(k^{\alpha+1})[1 + o(1)]$. The velocity of the particle is given by

$$
v_k(n) = \mathcal{I}_{\{n<k\}} - (-1)^{n-k}\mathcal{I}_{\{n\geqslant k\}}, \quad (14)
$$

where $\mathcal{I}_A$ is the indicator of the event A. Then by using Eq. (14) in Eq. (13), the moments of velocity switch between even and odd values of p. The even moments of velocity scale asymptotically like

$$
\langle v^p(n) \rangle \sim 1, \quad \text{as } n \to \infty, \quad \text{even } p \geqslant 2. \quad (15a)
$$

The odd $p \geqslant 1$ moments of velocity scale asymptotically as

$$
\langle v^p(n) \rangle \sim \begin{cases} 1 - 4R_\alpha, & \text{for even } n, \\ -1 + 4R_\alpha, & \text{for odd } n, \end{cases} \quad (15b)
$$

as n changes between even and odd values, where

$$
R_\alpha = \sum_{k=1}^{\infty} \Delta_{2k}(\alpha).
$$

5. Velocity autocorrelation function

The velocity of any point of the SM is either $+1$ or -1, and its autocorrelation is defined by

$$
\langle v(n_1)v(n_2) \rangle = 2 \sum_{k=1}^{n} v(n_1)v_k(n_2)\Delta_k(\alpha) + 2 \sum_{k=n+1}^{\infty} v(n_1)v_k(n_2)\Delta_k(\alpha), \quad (16)
$$

where $v_k(l)$, the velocity at time l of a particle with position $x \in [\ell_{k-1}^+, \ell_k^+)$, is given in Eq. (14). For $n_1 = 0$, we have $v(0) = 1$; hence

$$
\langle v(0)v(n_2) \rangle = 2 \sum_{k=1}^{n} v_k(n_2)\Delta_k(\alpha) + 2 \sum_{k=n_2+1}^{\infty} v_k(n_2)\Delta_k(\alpha). \quad (17)
$$

Calculations analogous to the previous ones now show that the velocity autocorrelation function oscillates asymptotically in n_2 between two values. Therefore velocity autocorrelation follows the same asymptotic scaling, Eq. (15b), as in the odd moments of velocity

$$
\langle v(0)v(n_2) \rangle \sim \langle v^p(n) \rangle, \quad \text{as } n \to \infty, \quad \text{odd } p \geqslant 1. \quad (18)
$$

The 2-times velocity autocorrelation function is also asymptotically split into two cases:

(i) when n_1 and n_2 are either both even or both odd, then

$$
\langle v(n_1)v(n_2) \rangle \to 1, \quad \text{as } n_1 \to \infty, \quad n_2 > n_1; \quad (19)
$$

(ii) when one of the two times is even and the other is odd, then

$$
\langle v(n_1)v(n_2) \rangle \to -1, \quad \text{as } n_1 \to \infty, \quad n_2 > n_1. \quad (20)
$$

B. The fly-and-die dynamics

In the FND dynamics, we label trajectories by their initial position, x_0. Until time $t_c(x_0)$ such a trajectory moves along the positive x axis with unit velocity. At time $t_c(x_0)$ it stops and remains at position $x_0 + t_c(x_0)$ for all later times. Accordingly, we call this FND dynamics. Its position at time t will be denoted as

$$
x(x_0, t) = \begin{cases} x_0 + t, & \text{for } t \leqslant t_c(x_0), \\ x_0 + t_c(x_0), & \text{for } t \geqslant t_c(x_0). \end{cases} \quad (21a)
$$

Superdiffusive motion is expected to emerge when the distribution of the times for the flights, $t_c(x_0)$, has a power-law tail. To be concrete, we consider here the case

$$
t_c(x_0) = \left(\frac{l}{x_0}\right)^{1/\mu}, \quad (21b)
$$

with initial conditions x_0 uniformly distributed in the interval $[0, 1]$, and $\mu > 0$. In the following, we explore the position and velocity moments and correlations of this ensemble of trajectories. The ensemble average is denoted by $\langle \cdot \rangle$. The probability $P(> t)$ to perform a flight longer than t amounts to the fraction of initial condition x_0 with $t_c(x_0) > t$ such that

$$
P(> t) = x_0(t) = \frac{l}{t^\mu}. \quad (22)
$$

1. pth position moments

Lemma 3. For $\mu > 0$, the *p*th position moment of the FND for the trajectories starting at initial position x_0 asymptotically scales as

$$
\langle |\Delta x(t)|^p \rangle \sim
\begin{cases}
\frac{\mu}{\mu - p} \, l^{p/\mu}, & \text{for } p < \mu, \\
l \, \ln \frac{t^\mu}{l}, & \text{for } p = \mu, \\
\frac{p \, l}{p - \xi} \, t^{p - \mu}, & \text{for } p > \mu.
\end{cases}
\tag{23}
$$

Proof. See Appendix A 2. ∎

In more detail, for a specific case $p = 2$, the MSD scales $\langle |\Delta x(t)|^2 \rangle \sim t^\gamma$, where $\gamma = 2 - \mu$ and $0 < \gamma < 2$. This exhibits a wide spectrum of diffusion: When the transport exponent $\gamma < 1$, this yields to subdiffusion; at $\gamma = 1$ this grows linearly in time (i.e., normal diffusion); and for $\gamma > 1$ it is superdiffusive. Thus the FND dynamics capture all the transport regimes computed for SM. The FND dynamics for $p > \mu$, when adopting $l \equiv 2$ and $\mu = \alpha$, capture all the position moments that are computed for the SM, Eq. (3).

2. Generalized position autocorrelation function

The generalized (or *n*-point) position autocorrelation function for the FND dynamics is defined as

$$
\begin{aligned}
\rho_\mu&(t_1, t_2, \ldots, t_n) \\
&= \langle \Delta x(t_1) \, \Delta x(t_2) \cdots \Delta x(t_n) \rangle \\
&= \langle [x(x_0, t_1) - x_0][x(x_0, t_2) - x_0] \cdots [x(x_0, t_n) - x_0] \rangle \\
&= \int_0^1 dx_0 [x(x_0, t_1) - x_0][x(x_0, t_2) - x_0] \\
&\quad \cdots [x(x_0, t_n) - x_0],
\end{aligned}
\tag{24}
$$

where it is assumed that $t_1 < t_2 < \cdots < t_n$. To evaluate the integral we follow the convention that t_n is always larger or equal to t_1. Accordingly, we split the integration range into n intervals:

$0 < x_0 < P(> t_n)$: The trajectories are still flying at time t_n such that $\Delta x(t_1) = t_1$, $\Delta x(t_2) = t_2, \ldots, \Delta x(t_{n-1}) = t_{n-1}$, $\Delta x(t_n) = t_n$.

$P(> t_n) < x_0 < P(> t_{n-1})$: The trajectories are still flying until time t_{n-1} but they have died by the time t_n. Consequently, $\Delta x(t_1) = t_1$, $\Delta x(t_2) = t_2, \ldots, \Delta x(t_{n-1}) = t_{n-1}$, and $\Delta x(t_n) = t_c(x_0)$.

⋮

$P(> t_1) < x_0 < 1$: The trajectories died before t_1. Consequently, $\Delta x(t_1) = \Delta x(t_2) = \cdots = \Delta x(t_n) = t_c(x_0)$.

Splitting the integral and performing a calculation allows us to interpret it as follows:

$$
\begin{aligned}
\rho_\mu(t_1, t_2, \ldots, t_n) &= (t_1 t_2 \cdots t_n) \int_0^{l/t_n^\mu} dx_0 \\
&\quad + (t_1 t_2 \cdots t_{n-1}) \int_{l/t_n^\mu}^{l/t_{n-1}^\mu} dx_0 \left(\frac{l}{x_0} \right)^{\frac{1}{\mu}} \\
&\quad + (t_1 t_2 \cdots t_{n-2}) \int_{l/t_{n-1}^\mu}^{l/t_{n-2}^\mu} dx_0 \left(\frac{l}{x_0} \right)^{\frac{2}{\mu}}
\end{aligned}
$$

$$
\begin{aligned}
&\quad + \cdots + \int_{l/t_1^\mu}^1 dx_0 \left(\frac{l}{x_0} \right)^{\frac{n}{\mu}} \\
&= \sum_{j=0}^n \left(\prod_{k=1}^{n-j} t_k \int_{l/t_{n-j+1}^\mu}^{l/t_{n-j}^\mu} dx_0 \left(\frac{l}{x_0} \right)^{\frac{j}{\mu}} \right).
\end{aligned}
\tag{25a}
$$

Simple integration allows us to write a general expression of the *n*-point position autocorrelation function as

$$
\rho_\mu(t_1, t_2, \ldots, t_n) = l \sum_{j=0}^n \prod_{k=1}^{n-j} t_k \left[\frac{\mu}{\mu - j} \left(t_{n-j}^{j-\mu} - t_{n-j+1}^{j-\mu} \right) \right],
\tag{25b}
$$

where $t_{n+1} = \infty$ and $t_0 = l^{1/\mu}$. When adopting $l \equiv 2$ and $\mu = \alpha$, correlation Eq. (25b) yields the same scaling as found for the *m*-point position autocorrelation of the SM, Eq. (6). Therefore the higher-order position autocorrelation function of the SM and the FND asymptotically scales in the same trend. Subsequently, we derive the 3-point position correlation function, upon setting $n = 3$ and performing calculations on Eq. (25b). Consequently, when $\mu \neq 1$, we find

$$
\begin{aligned}
\rho_\mu(t_1, t_2, t_3) \simeq\ & \frac{l \, t_1 t_2 t_3^{1-\mu}}{1 - \mu} - \frac{l \, \mu \, t_1 t_2^{2-\mu}}{(2 - \mu)(1 - \mu)} \\
& - \frac{l \, \mu \, t_1^{3-\mu}}{(2 - \mu)(3 - \mu)}.
\end{aligned}
\tag{26}
$$

(I) At a fixed time t_1, when considering two equivalent subsequent times t_2 and t_3, the MSD [cf. Eq. (23) with $p = 2$] exhibits an asymptotic scaling,

$$
\langle |\Delta x(t)|^2 \rangle \sim \frac{2 \, l}{2 - \alpha} t^{2-\mu}, \quad 0 < \mu < 2.
\tag{27}
$$

(II) For $t_1 = t_2 = t_3$, this reduces to the third moment for the displacement, Eq. (23), with $p = 3$,

$$
\langle |\Delta x(t)|^3 \rangle = \frac{3 \, l}{3 - \mu} t^{3-\mu}, \quad 0 < \mu < 3.
\tag{28}
$$

Some functional relationships between the times are defined as follows:

(1) varying t_1, t_2, and t_3 while keeping a fixed time lag, with $h_1 = t_2 - t_1$ and $h_2 = t_3 - t_2$;

(2) varying t_1 while setting $t_2 = t_1 + t_1^{q_1}$ and $t_3 = t_1 + t_1^{q_1} + t_1^{q_2}$ for some fixed value of $q_1 < 1$ and $q_2 < 1$;

(3) keeping $t_1 \leqslant t_2$ fixed while setting t_3 to vary.

Like the SM, when all n values approach infinity for the 3-point position autocorrelation function $\rho_\mu(t_1, t_2, t_3)$, as defined in Eq. (26), the power-law exponent exhibits the same scaling behavior as that found for the third position moment (see Lemma 2 for the case where $m = 3$). To better understand this, we need to look at how the correlation $\rho_\mu(n_1, n_1 + h_1, n_1 + h_1 + h_2)$ behaves when n_1 is very large. In this context, for large n_1, if the time lags h_{k-1} (for $k = 2, 3$) are either constant or grow as n^q with $q < 1$, the differences between the three times n_1, $n_1 + h_1$, and $n_1 + h_1 + h_2$ become insignificant compared to the average value of n_1. This means that as n_1 increases, the relative differences between these times diminish, leading to a simpler scaling relationship for the correlation function.

Lemma 4. For $0 < \mu < n$, as all t times tend to infinity and $h_{k-1} = t_k - t_{k-1}$, for $k = 2, 3, \ldots, n$, where h_{k-1} is either fixed or $\sim t_1^q$, with $q < 1$, the n-point position autocorrelation function ρ_μ as represented in Eq. (26) asymptotically scales as

$$\rho_\mu(t_1, t_2, \ldots, t_n) \sim \frac{n\,l}{n - \mu} t_1^{n-\mu}, \quad 0 < \mu < n. \quad (29)$$

Proof. This follows directly from Eq. (26). ∎

Remark 2. For $0 < \mu < n$, with $n = 2, 3$ when all times t tend to infinity, the 2- and 3-point position autocorrelation functions ρ_μ, following the h_{k-1} represented in Lemma 4, have the same asymptotic scaling, Eq. (29), as for the second, i.e., MSD, Eq. (27), and third moments of displacement, Eq. (28), i.e.,

$$\rho_\mu(t_1, t_2) \sim \langle |\Delta x(t)|^2 \rangle, \quad \text{and} \quad \rho_\mu(t_1, t_2, t_3) \sim \langle |\Delta x(t)|^3 \rangle, \quad (30)$$

respectively.

Therefore, it is observed that when time is significantly large, the position moments and correlation function of the SM and the FND scale in the same way. Like the SM, a single-parameter-dependent scaling of the correlation function, reconsider Eq. (26) and perform calculations, introducing the time lag $h_2 = t_3 - t_2$ and $h_1 = t_2 - t_1$, and normalizing by the factor $t_1 t_2^{2-\mu}$; the position autocorrelation as a function of h_2/t_2 is entailed as

$$\rho_\mu\left(\frac{h_2}{t_2}\right) = \frac{\phi_\mu(t_1, t_2, t_3)}{t_1 t_2^{2-\mu}} \simeq \frac{l}{1 - \mu}\left[\left(1 + \frac{h_2}{t_2}\right)^{1-\mu} - \frac{\mu}{2 - \mu}\right.$$
$$\left. - \frac{\mu(1 - \mu)}{(2 - \mu)(3 - \mu)}\left(1 + \frac{h_1}{t_1}\right)^{-(2-\mu)}\right], \quad \mu \neq 1. \quad (31a)$$

In the large time limit the asymptotic scaling for large and small values of h_2/t_2 and h_1/t_1 for $\mu < 1$ yields as

$$\rho_\mu\left(\frac{h_2}{t_2}\right) \simeq \begin{cases} \frac{l}{1-\mu}\left(\frac{h_2}{t_2}\right)^{1-\mu}, & \text{for} \quad h_2 \gg t_2, \\ \frac{3l}{3-\mu}, & \text{for} \quad h_2 \ll t_2, \; h_1 \ll t_1, \\ \frac{2l}{2-\mu}, & \text{for} \quad h_2 \ll t_2, \; h_1 \gg t_1. \end{cases} \quad (31b)$$

This scaling is identical to the SM expression when $l \equiv 2$, Eq. (12b), for large and small times. Therefore the asymptotic scaling of the 3-point position correlation as a function of h_2/t_2, the SM, and the FND scale in a similar fashion [cf. Eqs. (12b) and (31b)]. Hence we can predict data collapse of the 3-point position correlation irrespective of the time relationship. In Sec. III C, we emphasize this fact by comparing the qualitative prediction with LLG [29,34,35].

3. Moments of velocity

In the FND dynamics, the velocity of each trajectory is $+1$; these flying trajectories contribute to the velocity moments where other trajectories stop $v = 0$ and do not contribute. Therefore only those trajectories will contribute that are still flying $v = 1$. The moments of the velocity $\langle v^p(t) \rangle$ are obtained as

$$\langle v^p(t) \rangle = \langle |v(x_o, t) - v_0|^p \rangle = \int_0^1 dx_0 \, |v(x_o, t) - v_0|^p$$
$$= \int_0^{P(>t)} dx_0 \, t^p = \int_0^{l/t^\mu} dx_0,$$

which asymptotically scales as

$$\langle v^p(t) \rangle \sim l\,t^{-\mu}, \quad p \geqslant \mu. \quad (32)$$

This behavior is not shared by the velocity moments of the SM, Eq. (15).

4. Velocity autocorrelation function

The velocity of each flying trajectory in the FND dynamics is $+1$. The trajectories are flying with the velocity $v = 1$, till they stop, $v = 0$. Therefore only those trajectories contribute to the velocity autocorrelation functions with $t_1 \leqslant t_2 \leqslant \cdots t_n$ that are still flying at time t_n. Thus denoting velocity correlation $\rho_v(t_1, t_2, \ldots, t_n)$, we obtain

$$\rho_v(t_1, t_2, \ldots, t_n)$$
$$= \langle \Delta v(t_1) \Delta v(t_2) \cdots \Delta v(t_n) \rangle$$
$$= \langle [v(x_0, t_1) - v_0][v(x_0, t_2) - v_0] \cdots [v(x_0, t_n) - v_0] \rangle$$
$$= \int_0^1 dx_0 [v(x_0, t_1) - v_0][v(x_0, t_2) - v_0] \cdots [v(x_0, t_n) - v_0]$$
$$= \int_0^{P(>t_n)} dx_0 [v(x_0, t_1) - v_0][v(x_0, t_2) - v_0]$$
$$\cdots [v(x_0, t_n) - v_0]$$
$$= \int_0^{l/t_n^\mu} dx_0,$$

and therefore the velocity autocorrelation asymptotically scales as

$$\rho_v(t_1, t_2, \ldots, t_n) \simeq l\,t_n^{-\mu}, \quad n > \mu, \quad (33)$$

where $t_n = t_{n-1} + h_{n-1}, n \in \{2, 3, \ldots\}$ and $h > 0$.

This exhibits the same power-law tail, $-\mu$, for any order of velocity correlation function; moreover velocity moments and correlation asymptotically scale in the same power-law behavior [cf. Eq. (32)]. For $n = 2$, we find the 2-point velocity correlation function $\rho_v(t_1, t_2) \simeq l\,t_1^{-\mu}$, $0 < \mu < 2$. This behavior is not shared by the 2-time velocity autocorrelation function of the SM [cf. Eqs. (19) or (20)], and thus can be used to distinguish the transport processes.

III. STOCHASTIC PROCESS

A. The Lévy-Lorentz gas

The LLG was introduced in Barkai and Fleurov [29] as a one-dimensional model for anomalous transport in semiconductor devices where diffusion arises from scattering at dislocations at fixed random positions. Subsequently, it has been investigated by many authors [34,35]. The LLG is a one-dimensional model that comprises ballistic flights between scatterers at fixed random positions. The distances d between

neighboring scatterers are independently and identically distributed random variables sampled from a Lévy distribution with probability density

$$\lambda(d) \equiv \frac{\xi}{d_0}\left(\frac{d}{d_0}\right)^{-(\xi+1)}, \quad d \in [d_0, \infty), \qquad (34)$$

where $\xi > 0$ and d_0 is the minimum distance between scatterers. A point particle moves ballistically with velocity $\pm v$ between the two consecutive scatterers when it hits a scatterer; then it is either transmitted or reflected by the probability $1/2$. Barkai *et al.* [34] calculated bounds for the MSD for equilibrium and nonequilibrium initial conditions. Subsequently, Burioni *et al.* [35] adopted some simplifying assumptions to find the asymptotic form for nonequilibrium conditions of all moments $\langle|d(t)|^p\rangle$ with $p > 0$:

$$\langle|d(t)|^p\rangle \sim \begin{cases} t^{\frac{p}{1+\xi}}, & \text{for } \xi < 1, \ p < \xi, \\ t^{\frac{p(1+\xi)-\xi^2}{1+\xi}}, & \text{for } \xi < 1, \ p > \xi, \\ t^{\frac{p}{2}}, & \text{for } \xi > 1, \ p < 2\xi - 1, \\ t^{\frac{1}{2}+p-\xi}, & \text{for } \xi > 1, \ p > 2\xi - 1. \end{cases} \qquad (35)$$

For the MSD, $p = 2$, this result implies

$$\langle d(t)^2\rangle \sim t^\eta, \quad \eta = \begin{cases} 2 - \frac{\xi^2}{(1+\xi)}, & \text{for } \xi < 1, \\ \frac{5}{2} - \xi, & \text{for } 1 \leqslant \xi < 3/2, \\ 1, & \text{for } 3/2 \leqslant \xi. \end{cases} \qquad (36)$$

Unlike the SM and the FND, which enjoy subdiffusive transport for $\alpha > 1$ and $\mu > 1$, respectively, the nonequilibrium initial conditions for the LLG only lead to superdiffusive ($0 < \xi < 3/2$) or diffusive ($\xi \geqslant 3/2$) regimes; subdiffusion is not expected.

The moments of the SM in its superdiffusive regime ($0 < \alpha < 1$) can be mapped to those of the LLG [24,48]. All moments of the SM, Eq. (3) [and so FND, Eq. (23)], scale like those conjectured and numerically validated for the LLG, Eq. (35), once the second moments do. This is the case if the following holds [cf. Eqs. (3) and (23)]:

$$\alpha = \mu = \begin{cases} \frac{\xi^2}{(1+\xi)}, & \text{for } 0 < \xi \leqslant 1, \\ \xi - \frac{1}{2}, & \text{for } 1 < \xi \leqslant \frac{3}{2}, \\ 1, & \text{for } \frac{3}{2} < \xi. \end{cases} \qquad (37)$$

When adopting this mapping all other moments of the SM, the FND, and the LLG agree with those of the LLG, Eq. (35). This means that Eq. (37) makes these processes asymptotically indistinguishable from the point of view of all position moments and the 2-point position autocorrelation function [42,48]. We thus now extend this equivalence to the 3-point position autocorrelation function and check whether the higher correlations differ or they follow the same equivalence agreement. The single dimensionless time ratio h_2/t_2 expressions for the 3-point correlations are calculated analytically for the SM and the FND [cf. Eqs. (12) and (31)]. This will then be compared to numerically estimated data for the LLG. For the position autocorrelation function in the LLG, there are no analytic results of any order, such as those of Burioni *et al.* [35] for the

moments. We numerically estimate the 3-point displacement correlation in Sec. III B 1.

Remark 3. For $t \to \infty$, the asymptotic behavior of the third moment of displacement of the LLG can be obtained by requesting $p = 3$ in Eq. (35); one finds

$$\langle d(t)^3\rangle \sim t^{\overline{\eta}}, \quad \overline{\eta} = \eta + 1. \qquad (38)$$

B. Generalized position autocorrelation function

We define the generalized (or *n*-point) position autocorrelation function of the LLG as follows,

$$\varphi_\xi(t_1, t_2, \ldots, t_n) = \mathbb{E}\left[d(t_1)\,d(t_2)\cdots d(t_n)\right], \qquad (39)$$

where $\mathbb{E}$ denotes the averages, first average over the particles and then on the given random scatterers realization. We intend to compare the asymptotic form of the position autocorrelation function with the SM and the FND.

Lemma 5. For $\xi > 0$, and all t's tending to infinity, the *n*-point position autocorrelation function φ_ξ, Eq. (39), of the LLG has the following asymptotic form,

$$\varphi_\xi(t_1, t_2, \ldots, t_n) \sim c(h_1, h_2, \ldots, h_{n-1})t_1^{\omega_p}, \qquad (40)$$

for $p = 2, \ldots, n$, where the h's represent the time difference, $c(h_1, h_2, \ldots, h_{n-1})$ denotes the prefactor, and ω_p is the power-law exponent for the respective order of the correlation function; this will be obtained by best fit to the data.

We intend to compare the asymptotic form of the 3-point position autocorrelation function with the SM and the FND. In what follows, we define the 3-point position correlation function of the LLG.

1. 3-point position autocorrelation

We define the 3-point position autocorrelation function of the LLG by requesting $n = 3$ in Eq. (39) as follows,

$$\varphi_\xi(t_1, t_2, t_3) = \mathbb{E}\left[d(t_1)\,d(t_2)\,d(t_3)\right], \qquad (41)$$

where $\mathbb{E}$ denotes the averages, first average over the particles and then on the given random scatterers realization. Since our aim is to check the asymptotic equivalence of the position autocorrelation function with the SM and the FND, we follow the same time composition as adopted in Sec. II A 3:

(1) $h_1 = t_2 - t_1$, as $h_1 > 0$ either finite or $h_1 \sim t_1^{q_1}$, $q_1 < 1$, and $t_1 \to \infty$;

(2) $h_2 = t_3 - t_2$, as $h_2 > 0$ either finite or $h_2 \sim t_1^{q_2}$, $q_2 < 1$, where $t_2 = t_1 + h_1$, and $t_1 \to \infty$;

(3) $t_1 \geqslant t_2$ are fixed and set $t_3 \to \infty$.

The asymptotic scaling form for the moments and the 2-point position correlation of the SM and the LLG have been tested [24,48], when α and ξ obey Eq. (37). In the following, we now verify the theoretical prediction of the 3-point position autocorrelation as a function of h_2/t_2 of the SM [Eq. (12)] and FND [Eq. (31)] with numerically estimated correlations of the LLG [Eq. (41)] that α, μ, and ξ obey the same relation [Eq. (37)]. The importance of single qualitative scaling predicts the data collapse of the LLG for small and large h_2/t_2.
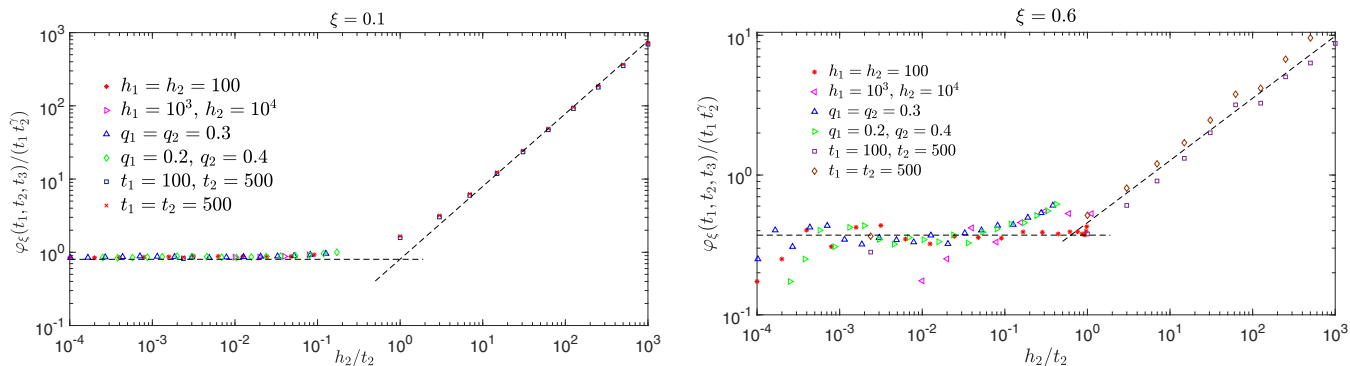
FIG. 2. The 3-point position autocorrelation functions $\varphi_\xi(t_1, t_2, t_3)$ of the LLG are plotted for $\xi = 0.1$ (left panel) and $\xi = 0.6$ (right panel). We obtain a data collapse for a vast data set of combinations of t_1, t_2, and t_3 by plotting the left-hand side of Eqs. (12) or (31) as a function of h_2/t_2. The different symbols denote data for $d_0 = 0.1$, where we varied the time t_1, while setting $t_2 = t_1 + h_1$ and $t_3 = t_1 + h_1 + h_2$, for h_1 and h_2 any positive constants (see legend) for the regime $h_2 < t_2$, and also we varied t_1 while setting $t_2 = t_1 + t_1^{q_1}$ and $t_3 = t_1 + t_1^{q_1} + t_1^{q_2}$ (see legend) for the regime $h_2 < t_2$. Similarly, for $h_2 > t_2$, keep $t_2 \geqslant t_1$ fixed and vary t_3 (see legend). The dashed lines show the parameter dependence Eq. (12) predicted by the SM [or so FND, Eq. (31)].

Remark 4. The asymptotic behavior of the 1-time velocity autocorrelation function of the LLG scales like $\langle v(0)\, v(t) \rangle \sim t^{-3/2}$, as obtained by Barkai *et al.* [29]; hence it can be used to distinguish the LLG from the SM and the FND dynamics.

C. Scaling test of the 3-point position autocorrelation function of the SM, FND, and LLG

In this section, we explore the equivalence of the 3-point position autocorrelation of the SM, the FND, and the LLG. We try here to extend this equivalence to the 3-point correlations, since the 2-point position correlation provides the faithful description of these systems [48]. We start by recalling the scaling of the 3-point position correlation represented in Eqs. (12) or (31) and see how far it captures the correlation of the LLG. We adopt different settings of time composition; in these settings, all data of different cases of correlation function sit on the same curve (see Fig. 2).

Data analysis

We have obtained a sufficient amount of numerically estimated data concerning the correlation function, exploring various relationships among the three time variables. In all these functional relationships between the times defined in Sec. III B 1, we find that the position autocorrelation function of the SM and the FND followed the dependence on Eqs. (12) or (31), and adopted the mapping of parameters α, μ, and ξ [cf. Eq. (37)]. This is demonstrated in Fig. 2, for the data collapse for one parameter-dependent 3-point position autocorrelation function with different functional relationships between three times. For $h_2 < t_2$, we observe an excellent match between the LLG data and quantitative prediction of the SM, Eq. (12), and the FND, Eq. (31), at least for small values of ξ. For $h_2 > t_2$, there is a different scaling and the agreement becomes gradually worse as ξ increases. The three times t_1, t_2, and t_3 are far separated for the asymptotic scaling of small h_2/t_2.

In Fig. 3, we represent the theoretical mapping of the SM (or so FND) and the LLG by their $(\xi; \alpha, \mu)$ relation shown in

Eq. (37). We also represent the fitted values for some ξ along the curve of the position moments and correlations. The position moment data are obtained by numerically estimating the power-law exponents η and $\overline{\eta}$ of the second moment $\langle d^2(t) \rangle$ and third moment $\langle d^3(t) \rangle$, respectively, and adopting $\mu(\xi) = \alpha(\xi) = 2 - \eta(\xi) \simeq 3 - \overline{\eta}(\xi)$. Likewise, the fitted values of the position correlations φ_ξ are obtained by estimating the power-law exponent of Eq. (40), ω_p, with $p = 2, 3$, where the exponents ω_2 and ω_3 render the 2- and 3-point position correlation functions, respectively, and adopting $\mu(\xi) = \alpha(\xi) = 2 - \omega_2 \simeq 3 - \omega_3$ [cf. Eqs. (11) and (30)]. The power-law scaling of the position autocorrelation function does the same as the asymptotic scaling of the position moment amounts with single time t (see Remark 2). These findings confirm the prediction of exponents provided by Eq. (37). Hence they can be used for the higher-order position moments and the correlation functions.
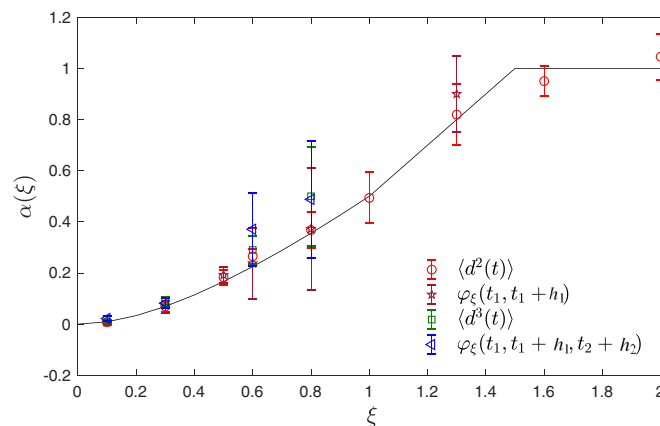
FIG. 3. This figure represents the parameters $(\xi; \alpha, \mu)$ functional relationship, Eq. (37), of the SM (or so FND) and the LLG, along with fitted values for some ξ. The fitted values with their bounds as a function of ξ for the position moments and the correlations of order $n = 2$ and $n = 3$ are obtained by the best fit to the data and adopting $\alpha(\xi) = n -$ best fit.

IV. DISCUSSION AND CONCLUSION

The investigation on the equivalence of observables between the SM and the LLG was started by Salari *et al.* [24], who observed that the moments scale in the same fashion. Since moments contain only partial information on the transport systems, knowledge of the correlation is an essential ingredient to highly characterize anomalous transport dynamics [30]. Therefore, Giberti *et al.* [48] derived the 2-point position autocorrelation function of the SM in several scaling forms and compared it with the numerically estimated position autocorrelation function of the LLG. They found a remarkable agreement in scaling, at least for lower scatterer density (i.e., for small values of ξ). Findings on the coincidence of the position moments and the 2-point position autocorrelation function are not a hallmark of the indistinguishability of these transport systems. Other observables are needed to distinguish these processes; for instance, the velocity autocorrelation functions of these processes are quite different.

In this paper, the general order position autocorrelation functions ϕ_α of the SM [Eq. (6)] and ρ_μ of the FND [Eq. (25)] are analytically computed. For a special case, their 3-point position autocorrelation functions are also presented. Based on these analytical expressions, a single scaling relation for the 3-point position autocorrelation function is established, allowing the representation of the correlation function in a scaling form where it only depends on the ratio of times h_2/t_2 [cf. Eqs. (12) and (31)]. The excellent agreement between the numerical data of the LLG and the predictions obtained by the SM and the FND (symbols and dashed lines in Fig. 2) establishes a new way to analyze correlations in anomalous transport. Additionally, it is argued that the position moments and correlations are posed in the same way, provided that the $(\xi; \alpha, \mu)$ relation follows Eq. (37), as represented in Fig. 3. It only depends on the exponent η characterizing the MSD and the prefactor of that asymptotic power law.

To conclude, at the very least, for small ξ, the 3-point position autocorrelation function of the SM and the FND can capture the main features of the correlation function for the nontrivial anomalous transport process. We argued that systems with different microscopic dynamics but enjoying the same transport properties, such as position moments and correlation functions up to order 3, should be considered. Consequently, for superdiffusive transport, the position moments and autocorrelation functions of the SM, the FND, and the LLG are dominated by ballistic trajectories. The behavior of rare events at large distances in the SM, the FND, and the LLG is determined by the same physical origin: a single ballistic jump. This is described in the general framework of a single big jump in [44,45]. This ballistic jump determines all the dynamical correlations when the diffusive parameters of these systems are small enough. Conversely, at short distances, the typical dynamical evolution differs significantly. The big jump principle holds not only for power-law distributions with small exponents but also in models characterized by subexponential distributions, as noted in [50]. However, when parameters such as α, μ, or ξ change, the big jump is observed in different observables. For instance, the big jump determines the correlation functions specifically for a power-law proba-

bility density function with a sufficiently small exponent. In the SM and the FND, the typical asymptotic dynamics are frozen; the trajectories become periodic within their neighboring cells in the SM and die in the FND. In contrast, for the LLG, the typical asymptotic dynamics can be diffusive or subdiffusive, depending on the value of ξ [45]. It is conjectured that the position moments and the autocorrelation function apply to a wide class of such systems [42]. Even with entirely different microscopic dynamics, the models agree regarding the characteristics of the displacement. However, the moments and correlations of the velocities may differ. In summary, these concepts have potential applications in various fields, ranging from dynamical systems and ecology to statistical physics, providing valuable insights into the behavior of complex systems.

APPENDIX: SUPPORTING DERIVATION FOR THE POSITION MOMENTS

1. Derivation for *p*th position moments of the SM

In this Appendix we show the derivation of *p*th position moments, which is represented in Lemma 1. The position moments are a function of the number n of iterations of the map S_α. For $n \gg 2^{1/\alpha}$ one obtains

$$\langle (x_n - x_0)^p \rangle \simeq 2 \int_0^{\ell_n} dx\, n^p + 2 \int_{\ell_n}^{1/2} dx\, (x^{-1/\alpha} - 2^{1/\alpha})^p$$

$$\simeq 2\, n^p\, \ell_n + \frac{2}{1 - p/\alpha} \left(2^{-1+p/\alpha} - \ell_n^{1-p/\alpha} \right) + \mathcal{O}(1)$$

$$\sim \frac{2\,p}{p - \alpha}\, n^{p-\alpha} + \mathcal{O}(1) \tag{A1}$$

$$\sim \begin{cases} \text{constant}, & \text{for } p < \alpha, \\ \frac{2\,p}{p-\alpha}\, n^{p-\alpha}, & \text{for } p > \alpha > 0, \end{cases} \tag{A2}$$

while for $p = \alpha$, Eq. (A1) leads to

$$\langle (x_n - x_0)^\alpha \rangle \sim 2\, \ln \frac{n^\alpha}{2}. \tag{A3}$$

Collecting terms from Eqs. (A2) and (A3) completes the proof of Lemma 1.

2. Derivation for *p*th position moments of the FND

This Appendix shows the derivation of *p*th moments of the FND; the asymptotic scaling is represented in Lemma 3. For $p = \mu$, the *p*th position moments can be obtained,

$$\langle |\Delta x(t)|^p \rangle = \langle |x(x_0, t) - x_0|^p \rangle$$

$$= \int_0^1 |x(x_0, t) - x_0|^p dx_0$$

$$= \int_0^{P(>t)} t^\mu\, dx_0 + \int_{P(>t)}^1 [t_c(x_0)]^\mu dx_0, \tag{A4}$$

where $t_c(x_0)$ is the final position of the particle and has a power-law tail, expressed in Eq. (21b). The probability $P(> t)$ to perform a flight longer than t amounts to the fraction of initial condition x_0 with $t_c(x_0) > t$ [cf. Eq. (22)], such that from Eqs. (21b) and (22), we can write Eq. (A4) as follows:

$$\langle |\Delta x(t)|^p \rangle = \int_0^{l/t^\mu} t^\mu \, dx_0 + \int_{l/t^\mu}^1 [t_c(x_0)]^\mu dx_0 = t^p \frac{l}{t^\mu} + \frac{l^{p/\mu}}{1 - p/\mu} \left[1 - \left(\frac{l}{t^\mu} \right)^{1 - p/\mu} \right]. \tag{A5}$$

Rearranging and collecting terms for the $t^{p-\mu}$ and $l^{p/\mu}$, one finds

$$\langle |\Delta x(t)|^p \rangle = \frac{pl}{p - \mu} t^{p-\mu} + \frac{\mu}{\mu - p} l^{p/\mu}.$$

Analogous derivation for $p = \mu$, and in the limit of long times $t > l^{1/\mu}$, completes the proof of Lemma 3.

---

[1] H. Scher and E. W. Montroll, Anomalous transit-time dispersion in amorphous solids, Phys. Rev. B **12**, 2455 (1975).

[2] O. G. Jepps, C. Bianca, and L. Rondoni, Onset of diffusive behavior in confined transport systems, Chaos **18**, 013127 (2008).

[3] O. G. Jepps and L. Rondoni, Thermodynamics and complexity of simple transport phenomena, J. Phys. A: Math. Gen. **39**, 1311 (2006).

[4] E. K. Lenzi, R. S. Zola, H. V. Ribeiro, D. S. Vieira, F. Ciuchi, A. Mazzulla, N. Scaramuzza, and L. R. Evangelista, Ion motion in electrolytic cells: Anomalous diffusion evidences, J. Phys. Chem. B **121**, 2882 (2017).

[5] E. Barkai, Y. Garini, and R. Metzler, Strange kinetics of single molecules in living cells, Phys. Today **65**(8), 29 (2012).

[6] Y. Sagi, M. Brook, I. Almog, and N. Davidson, Observation of anomalous diffusion and fractional self-similarity in one dimension, Phys. Rev. Lett. **108**, 093002 (2012).

[7] S. Havlin and D. Ben-Avraham, Diffusion in disordered media, Adv. Phys. **51**, 187 (2002).

[8] J.-H. Jeon, N. Leijnse, L. B. Oddershede, and R. Metzler, Anomalous diffusion and power-law relaxation of the time averaged mean squared displacement in worm-like micellar solutions, New J. Phys. **15**, 045011 (2013).

[9] J.-H. Jeon, H. M.-S. Monne, M. Javanainen, and R. Metzler, Anomalous diffusion of phospholipids and cholesterols in a lipid bilayer and its origins, Phys. Rev. Lett. **109**, 188103 (2012).

[10] J. Szymanski and M. Weiss, Elucidating the origin of anomalous diffusion in crowded fluids, Phys. Rev. Lett. **103**, 038102 (2009).

[11] N. Gal and D. Weihs, Experimental evidence of strong anomalous diffusion in living cells, Phys. Rev. E **81**, 020903(R) (2010).

[12] D. Froemberg, M. Schmiedeberg, E. Barkai, and V. Zaburdaev, Asymptotic densities of ballistic Lévy walks, Phys. Rev. E **91**, 022131 (2015).

[13] R. M. Feliczaki, E. Vicentini, and P. P. González-Borrero, Dynamical transition on the periodic Lorentz gas: Stochastic and deterministic approaches, Phys. Rev. E **96**, 052117 (2017).

[14] R. Klages, G. Radons, and I. M. Sokolov, editors, *Anomalous Transport: Foundations and Applications* (Wiley-VCH, Weinheim, Germany, 2008).

[15] W. Wang, A. G. Cherstvy, R. Metzler, and I. M. Sokolov, Restoring ergodicity of stochastically reset anomalous-diffusion processes, Phys. Rev. Res. **4**, 013161 (2022).

[16] R. Metzler and J. Klafter, The random walk's guide to anomalous diffusion: A fractional dynamics approach, Phys. Rep. **339**, 1 (2000).

[17] R. Metzler and J. Klafter, The restaurant at the end of the random walk: Recent developments in the description of anomalous transport by fractional dynamics, J. Phys. A: Math. Gen. **37**, R161 (2004).

[18] R. Klages, *Microscopic Chaos, Fractals and Transport in Nonequilibrium Statistical Mechanics* (World Scientific, Singapore, 2007).

[19] R. Metzler, J.-H. Jeon, A. G. Cherstvy, and E. Barkai, Anomalous diffusion models and their properties: Non-stationarity, non-ergodicity, and ageing at the centenary of single particle tracking, Phys. Chem. Chem. Phys. **16**, 24128 (2014).

[20] P. Gaspard, *Chaos, Scattering and Statistical Mechanics* (Cambridge University Press, Cambridge, 1998).

[21] J. R. Dorfman, *An Introduction to Chaos in Non-Equilibrium Statistical Mechanics* (Cambridge University Press, Cambridge, 1999).

[22] R. Klages, *Deterministic Diffusion in One-Dimensional Chaotic Dynamical Systems* (Wissenschaft & Technik-Verlag, Berlin, 1996).

[23] O. G. Jepps, S. K. Bathia, and D. J. Searles, Wall mediated transport in confined spaces: Exact theory for low density, Phys. Rev. Lett. **91**, 126102 (2003).

[24] L. Salari, L. Rondoni, C. Giberti, and R. Klages, A simple non-chaotic map generating subdiffusive, diffusive, and superdiffusive dynamics, Chaos **25**, 073113 (2015).

[25] G. M. Zaslavsky, Chaos, fractional kinetics, and anomalous transport, Phys. Rep. **371**, 461 (2002).

[26] C. P. Dettmann and E. G. D. Cohen, Microscopic chaos and diffusion, J. Stat. Phys. **101**, 775 (2000).

[27] F. Cecconi, D. del Castillo-Negrete, M. Falcioni, and A. Vulpiani, The origin of diffusion: The case of non-chaotic systems, Physica D **180**, 129 (2003).

[28] T. Geisel, J. Nierwetberg, and A. Zacherl, Accelerated diffusion in Josephson junctions and related chaotic systems, Phys. Rev. Lett. **54**, 616 (1985).

[29] E. Barkai and V. Fleurov, Stochastic one-dimensional Lorentz gas on a lattice, J. Stat. Phys. **96**, 325 (1999).

[30] I. M. Sokolov, Models of anomalous diffusion in crowded environments, Soft Matter **8**, 9043 (2012).

[31] G. M. Zaslavsky, *The Physics of Chaos in Hamiltonian Systems*, 2nd ed. (Department of Physics & Courant Institute of Mathematical Sciences, New York University, USA, 2007).

[32] S. Denisov, J. Klafter, and M. Urbakh, Dynamical heat channels, Phys. Rev. Lett. **91**, 194301 (2003).

[33] B. Li, J. Wang, L. Wang, and G. Zhang, Anomalous heat conduction and anomalous diffusion in nonlinear lattices, single walled nanotubes, and billiard gas channels, Chaos **15**, 015121 (2005).

[34] E. Barkai, V. Fleurov, and J. Klafter, One-dimensional stochastic Lévy-Lorentz gas, Phys. Rev. E **61**, 1164 (2000).

[35] R. Burioni, L. Caniparoli, and A. Vezzani, Lévy walks and scaling in quenched disordered media, Phys. Rev. E **81**, 060101(R) (2010).

[36] Y. Liang, W. Wang, R. Metzler, and A. G. Cherstvy, Anomalous diffusion, nonergodicity, non-Gaussianity, and aging of fractional Brownian motion with nonlinear clocks, Phys. Rev. E **108**, 034113 (2023).

[37] W. Wang, A. G. Cherstvy, X. Liu, and R. Metzler, Anomalous diffusion and nonergodicity for heterogeneous diffusion processes with fractional Gaussian noise, Phys. Rev. E **102**, 012146 (2020).

[38] V. Y. Zaburdaev, Microscopic approach to random walks, J. Stat. Phys. **133**, 159 (2008).

[39] A. Baule and R. Friedrich, A fractional diffusion equation for two-point probability distributions of a continuous-time random walk, Europhys. Lett. **77**, 10002 (2007).

[40] E. Barkai and I. M. Sokolov, Multi-point distribution function for the continuous time random walk, J. Stat. Mech.: Theory Exp. (2007) P08001.

[41] V. Zaburdaev, S. Denisov, and J. Klafter, Lévy walks, Rev. Mod. Phys. **87**, 483 (2015).

[42] J. Vollmer, L. Rondoni, M. Tayyab, C. Giberti, and C. M.-Monasterio, Displacement autocorrelation functions for strong anomalous diffusion: A scaling form, universal behavior, and corrections to scaling, Phys. Rev. Res. **3**, 013067 (2021).

[43] P. Castiglione, A. Mazzino, P. Muratore-Ginanneschi, and A. Vulpiani, On strong anomalous diffusion, Physica D **134**, 75 (1999).

[44] A. Vezzani, E. Barkai, and R. Burioni, Single-big-jump principle in physical modeling, Phys. Rev. E **100**, 012108 (2019).

[45] A. Vezzani, E. Barkai, and R. Burioni, Rare events in generalized Lévy walks and the big jump principle, Sci. Rep. **10**, 2732 (2020).

[46] A. Bianchi, G. Cristadoro, M. Lenci, and M. Ligabò, Random walks in a one-dimensional Lévy random environment, J. Stat. Phys. **163**, 22 (2016).

[47] M. Zamparo, Large fluctuations and transport properties of the Lévy-Lorentz gas, Ann. Inst. H. Poincar Probab. Statist. **59**, 621 (2023).

[48] C. Giberti, L. Rondoni, M. Tayyab, and J. Vollmer, Equivalence of position-position auto-correlations in the slicer map and the Lévy-Lorentz gas, Nonlinearity **32**, 2302 (2019).

[49] D. M.- Garcia, T. Sandev, H. Safdari, G. Pagnini, A. Chechkin, and R. Metzler, Crossover from anomalous to normal diffusion: truncated power-law noise correlations and applications to dynamics in lipid bilayers, New J. Phys. **20**, 103027 (2018).

[50] R. Burioni and A. Vezzani, Rare events in stochastic processes with sub-exponential distributions and the big jump principle, J. Stat. Mech.: Theory Exp. (2020) 034005.

[51] See http://hpc.polito.it.